The Astrophysical Journal Letters, 748:L21 (6pp), 2012 April 1 doi:10.1088/2041-8205/748/2/L21

FIRST RESULTS FROM $Z-$FOURGE*: DISCOVERY OF A CANDIDATE CLUSTER AT $z = 2.2$ IN COSMOS

Lee R. Spitler[1], Ivo Labbé[2,3], Karl Glazebrook[1], S. Eric Persson[2], Andy Monson[2], Casey Papovich[4], Kim-Vy H. Tran[4], Gregory B. Poole[1], Ryan Quadri[2,6], Pieter van Dokkum[5], Daniel D. Kelson[2], Glenn G. Kacprzak[1,7], Patrick J. McCarthy[2], David Murphy[2], Caroline M. S. Straatman[3], and Vithal Tilvi[4]
[1] Centre for Astrophysics & Supercomputing, Swinburne University, Hawthorn, VIC 3122, Australia; lspitler@astro.swin.edu.au
[2] Carnegie Observatories, Pasadena, CA 91101, USA
[3] Sterrewacht Leiden, Leiden University, NL-2300 RA Leiden, The Netherlands
[4] George P. and Cynthia Woods Mitchell Institute for Fundamental Physics and Astronomy, and Department of Physics and Astronomy, Texas A&M University, College Station, TX, 77843-4242, USA
[5] Department of Astronomy, Yale University, New Haven, CT 06520, USA
Received 2011 December 12; accepted 2012 February 15; published 2012 March 12

ABSTRACT

We report the first results from the $Z-$FOURGE survey: the discovery of a candidate galaxy cluster at $z = 2.2$ consisting of two compact overdensities with red galaxies detected at $\gtrsim 20\sigma$ above the mean surface density. The discovery was made possible by a new deep ($K_s \lesssim 24.8$ AB 5σ) Magellan/FourStar near-IR imaging survey with five custom medium-bandwidth filters. The filters pinpoint the location of the Balmer/4000 Å break in evolved stellar populations at $1.5 < z < 3.5$, yielding significantly more accurate photometric redshifts than possible with broadband imaging alone. The overdensities are within $1'$ of each other in the COSMOS field and appear to be embedded in a larger structure that contains at least one additional overdensity ($\sim 10\sigma$). Considering the global properties of the overdensities, the $z = 2.2$ system appears to be the most distant example of a galaxy cluster with a population of red galaxies. A comparison to a large ΛCDM simulation suggests that the system may consist of merging subclusters, with properties in between those of $z > 2$ protoclusters with more diffuse distributions of blue galaxies and the lower-redshift galaxy clusters with prominent red sequences. The structure is completely absent in public optical catalogs in COSMOS and only weakly visible in a shallower near-IR survey. The discovery showcases the potential of deep near-IR surveys with medium-band filters to advance the understanding of environment and galaxy evolution at $z > 1.5$.

Key words: galaxies: clusters: general – galaxies: high-redshift – large-scale structure of universe

1. INTRODUCTION

Galaxy clusters are the most overdense cosmological regions in the universe and are unique astronomical tools: their abundance constrains fundamental cosmological parameters and they provide an extreme laboratory for elucidating the role of local environment in the evolution of the massive galaxies.

However, despite extensive multi-wavelength searches, only a few evolved galaxy clusters with red galaxies have been found at $z \gtrsim 1.5$ (e.g., McCarthy et al. 2007; Andreon et al. 2009; Papovich et al. 2010; Tanaka et al. 2010; Fassbender et al. 2011; Gobat et al. 2011; Santos et al. 2011). More diffuse protoclusters of star-forming galaxies have been found to higher redshift (e.g., Steidel et al. 2000; Venemans et al. 2007; Capak et al. 2011), although it is unclear how they relate to lower-redshift massive clusters.

Ideally, we want to find massive distant structures using spectroscopy. The problem is that most cluster galaxies at $z > 1.5$ are too faint for spectroscopy, while photometric redshifts derived from broadband photometry are generally not accurate enough for secure identification. A novel approach is to use near-infrared imaging with *medium-bandwidth* filters, which are narrower than traditional broadband filters and provide significantly more accurate photometric redshifts (e.g., $\delta z/(1+z) \sim 1\%$–2% at $z \sim 2$; van Dokkum et al. 2009; Whitaker et al. 2011) for thousands of sources simultaneously over large contiguous fields of view (e.g., Wolf et al. 2003).

Using the newly commissioned FourStar near-IR camera (Persson et al. 2008) on the 6.5 m Magellan Baade Telescope, we have initiated a major survey to obtain deep medium-bandwidth near-IR imaging over several fields. Our custom filters span $1.0\,\mu$m–$1.8\,\mu$m and hence trace the Balmer/4000 Å break in galaxies at $1.5 < z < 3.5$. The FourStar Galaxy Evolution Survey ($Z-$FOURGE)[8] will be described in detail by I. Labbé et al. (2012, in preparation). This Letter demonstrates that the improved depth and redshift accuracies allow us to search for massive galaxy overdensities at redshifts $z \gtrsim 1.5$.

2. OBSERVATIONS AND ANALYSIS

As part of the ongoing survey we observed a single $\approx 11' \times 11'$ pointing within the COSMOS field (Scoville et al. 2007) with Magellan/FourStar in the spring of 2011, imaging for 41 hr in five medium-bandwidth filters (J_1, J_2, J_3, H_s, H_l) and the broadband K_s filter to 5σ point-source limiting depths ($D = 1.''5$ aperture corrected to total) of 25.5, 25.4, 25.3, 24.8, 24.7, and 24.8 AB mag, respectively. Raw images were processed using our custom pipeline, also used for the NEWFIRM Medium Band Survey (NMBS; Whitaker et al. 2011).

`SExtractor` (Bertin & Arnouts 1996) was used to select objects in the K_s image (FWHM $\approx 0.''40$; $0.''15$ pixel^{-1}) to a depth of $K_s \sim 24.5$ and to extract $D = 1.''5$ aperture fluxes from point-spread-function-matched versions of our $Z-$FOURGE COSMOS data, plus 23 optical and 4 *Spitzer*/IRAC COSMOS

* This Letter includes data gathered with the 6.5 m Magellan Telescopes located at Las Campanas Observatory, Chile.
[6] Hubble Fellow.
[7] Australian Research Council Super Science Fellow.
[8] http://z-fourge.strw.leidenuniv.nl

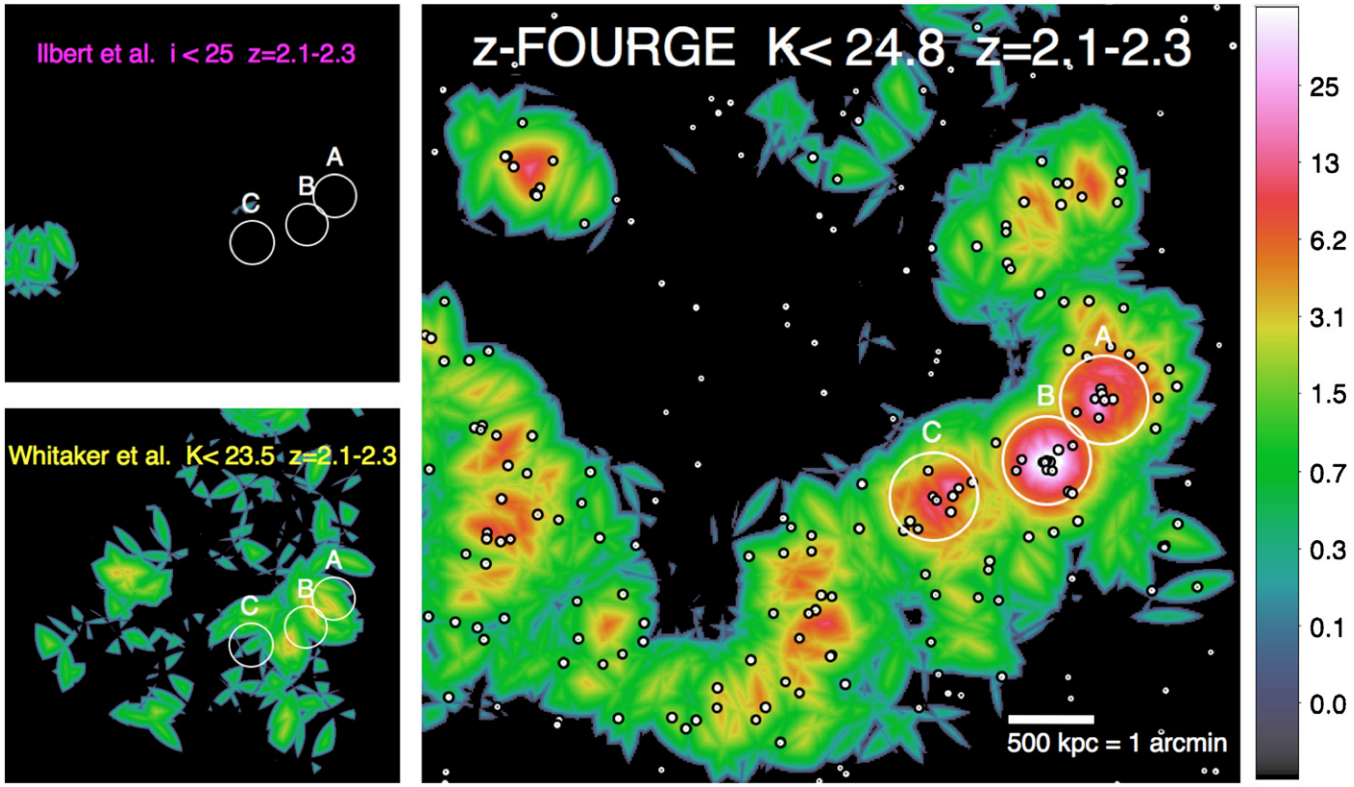

Figure 1. Seventh nearest-neighbor surface density maps for $z = 2.1$–2.3 in a $\approx 9' \times 9'$ region in the COSMOS field. Units are standard deviations above the mean. Density maps, including those from literature photometric redshift catalogs (Ilbert et al. 2009; Whitaker et al. 2011), are labeled along with the limiting selection magnitude. Individual $Z-$FOURGE galaxies at $z = 2.1$–2.3 are represented by small circles. The maps illustrate the advantage of deep near-infrared imaging with medium-band filters for finding large-scale structures at $z \sim 2$.

legacy image sets. Photometric zero points were calibrated using sources in common with the NMBS catalog in COSMOS (Whitaker et al. 2011). We adopt the AB magnitude system and a cosmology with $H_0 = 70$ km s^{-1} Mpc^{-1}, $\Omega_m = 0.3$, and $\Omega_\Lambda = 0.7$. Stars were culled using a $U - J_1$ and $J_1 - K_s$ color–color criterion (Whitaker et al. 2011).

We derived photometric redshifts with EAZY (Brammer et al. 2008) and fitted Bruzual & Charlot (2003, hereafter BC03) stellar population models using FAST (Kriek et al. 2009), assuming exponentially declining star formation histories, solar metallicity, and a Chabrier (2003) initial mass function. We note that photometric redshifts derived with similar near-IR medium-band filters yielded a normalized median absolute deviation of $\delta_{z,\mathrm{nmad}}/(1+z) = 2\%$ at $z = 1.7$–2.7 in the NMBS survey (van Dokkum et al. 2009).

3. OVERDENSITIES AT $z = 2.2$

3.1. Discovery

We searched for high-redshift galaxy overdensities by computing surface density maps in narrow $\delta z = 0.2$ redshift slices between $z = 1.5$–3.5 using the seventh nearest-neighbor metric (e.g., Papovich et al. 2010; Gobat et al. 2011). At each location in the map, we calculate the projected distance to the seventh nearest neighbor and evaluate the projected density $n_7 = N/(\pi * r_N^2)$. The results do not change significantly for density maps with $N = 5$–9.

As shown in Figure 1, a system consisting of three strong galaxy overdensities within a radius of 1.′5 was found between $z = 2.1$–2.3. At these redshifts the Balmer/4000 Å break passes through the FourStar $J_1(1.05\,\mu\mathrm{m})$, $J_2(1.15\,\mu\mathrm{m})$, and $J_3(1.28\,\mu\mathrm{m})$ medium-band filters. Figure 2 shows images of the overdensities, which each contain dense concentrations of galaxies with red $J_2 - J_3$ colors, consistent with the presence of prominent Balmer/4000 Å breaks at $z \sim 2.2$.

Figure 3 presents photometric redshifts for the overdensity galaxies and further confirms that they are strongly peaked at $z \approx 2.2$. The overdensities have consistent mean redshifts ($z^{\mathrm{A}} = 2.16 \pm 0.03$, $z^{\mathrm{B}} = 2.19 \pm 0.03$, $z^{\mathrm{C}} = 2.21 \pm 0.03$; uncertainties are random error on the mean) and together show a weighted mean of 2.19 ± 0.03 (here we adopt as the uncertainty the range of the three overdensity redshifts). The rms scatter of individual galaxies is 0.06 or $\delta z/(1+z) = 0.02$. There are 7, 13, and 9 candidate members within $<30''$ of the overdensities[9] A, B, and C, respectively. The red objects furthermore have steep Balmer/4000 Å breaks between the J_2 and J_3 filters, as shown in Figure 4.

We also calculated a density map using existing photometric redshift catalogs in COSMOS (Ilbert et al. 2009; Whitaker et al. 2011) in Figure 1. The overdensities are completely absent in the public i-band selected catalog of Ilbert et al. (2009). Only a weak impression of the overdensities is apparent in the K_s-band selected catalog of Whitaker et al. (2011). This substantiates the critical role that deep, near-IR imaging with medium-band filters will play in understanding environment and galaxy evolution at redshifts $z > 1.5$.

[9] We adopt the brightest galaxy as an overdensity's center: (10:00:15.753, +02:15:39.56), (10:00:18.380, +02:14:58.81), and (10:00:23.552, +02:14:34.13) for overdensities A, B, and C, respectively (J2000).

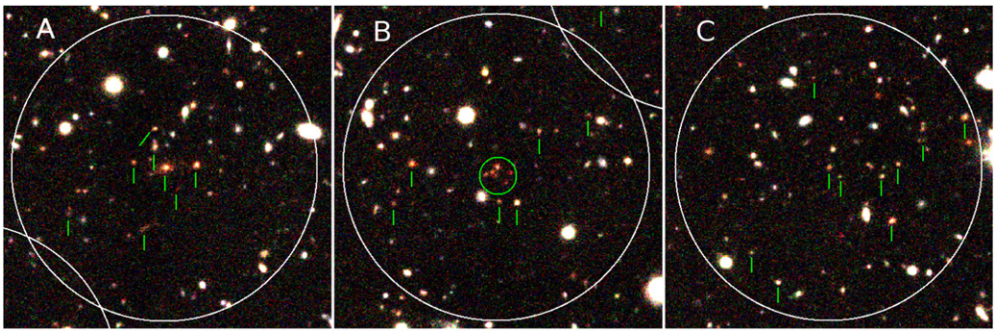

Figure 2. Color composite images in the J_1 (blue, 1.05 μm), J_2 (green, 1.15 μm), and J_3 (red, 1.28 μm) $\Delta\lambda/\lambda \sim 10\%$ filters, centered on each overdensity in the $Z-$FOURGE observations with FourStar in the COSMOS field. Galaxies at $z = 2.0$–2.3 with strong Balmer/4000 Å breaks have red colors in this image and are marked with green symbols. White circles have $r = 30''$.

We note that the candidate cluster satisfies the *Spitzer*/IRAC color based selection criteria of Papovich (2008) used to discover a $z = 1.62$ cluster (Papovich et al. 2010). However, unlike the IRAC selection, our catalogs provide accurate photometric redshifts, thus reducing spurious detections from foreground interlopers and enabling the secure identification of an overdensity at $z \sim 2.2$.

3.2. Significance of the Overdensities

To quantify the statistical significance of the overdensities, we first estimated the mean and intrinsic scatter in the nearest-neighbor density map of Figure 1. To avoid biasing these values by the strong overdensities themselves, we use the mean density ($n_7 = 2.6$ arcmin^{-2}) and its standard deviation ($\sigma_{n7} = 1.4$ arcmin^{-2}) from adjacent redshift slices ($z = 1.9$–2.1 and $z = 2.3$–2.5). These statistics reflect the distribution of nearest-neighbor densities evaluated only at the locations of all galaxies in a redshift slice. We find that the overdensities are $\approx 20\sigma$, 50σ, and 10σ deviations for A, B, and C, respectively.

We also performed a bootstrap resampling of the FourStar redshifts. At each instance, we shuffled all redshifts in our catalog and generated a seventh nearest-neighbor density map. To robustly identify overdensities in the resampled maps, we tuned `SExtractor` (`DETECT_THRESH`, `SEEING_FWHM`) to detect only overdensities A and B in the real density map. In only 3 of the 1000 resampled maps was *a single* overdensity detected. When tuned to find the less significant overdensity C, `SExtractor` detects only 65 overdensities in the resampled maps. Note that the number of valid analogs in the resampled maps would decrease further if we tried to match the tight spatial configuration of the real overdensities.

As a final check, we analyzed 121 mock density maps from simulated light cones produced by the Mock Galaxy Factory (M. Bernyk et al. 2012, in preparation). These are based upon the Millennium Simulation (Springel et al. 2005) and semi-analytical models of Croton et al. (2006). After introducing fake redshift errors, we matched the number of observed galaxies in the $Z-$FOURGE COSMOS field by selecting an R-band absolute magnitude limit $M_R < -21.6$ (roughly $K_s \lesssim 24.5$ at $z = 2.2$) and found a consistent scatter ($\sigma_{n7} = 2.0 \pm 0.7$ arcmin^{-2}) with our own estimate.

The above results confirm that overdensities A and B are robust, while overdensity C appears to be slightly less significant. Its close proximity to A and B raises the intriguing possibility that it is associated with the AB system. We therefore include overdensity C in the following.

4. CANDIDATE CLUSTER PROPERTIES

4.1. Galaxy Properties

Of the 313 galaxies in the redshift slice $2.1 \leqslant z \leqslant 2.3$ over the full $Z-$FOURGE COSMOS field, 29 galaxies are within $30''$ of a $z = 2.2$ overdensity. We consider these candidate overdensity galaxies.

Figure 5 shows the observed color–magnitude diagrams for all galaxies having $2.1 \leqslant z \leqslant 2.3$. The $J_1 - H_l$ color probes continuum on both sides of the 4000 Å break and avoids rest-frame Hα in K_s. The histograms in Figure 5 show that the non-overdensity or "field" distribution is dominated by blue galaxies ($J_1 - H_l < 1.6$) while the overdensity galaxies have a higher fraction of red galaxies.

We calculated the red galaxy fractions, $f_{\rm red} = N_{\rm red}/N_{\rm total}$, of each overdensity. Here $N_{\rm red}$ is the number of galaxies with $J_1 - H_l \geqslant 1.6$ at *all* magnitudes within $r < 30''$ of an overdensity at $2.1 \leqslant z \leqslant 2.3$. Apart from C ($f_{\rm red} = 0.2 \pm 0.2$), the two main overdensities show somewhat higher red galaxy fractions (together $f_{\rm red} = 0.5 \pm 0.2$) compared to the field population ($f_{\rm red} = 0.20 \pm 0.03$; $f_{\rm red}$ errors reflect counting statistics only).

Figure 5 shows that the red galaxies have similar colors to BC03 single-burst stellar population models at $z = 2.2$ and formation redshifts of $z_{\rm form} \gtrsim 3$. Fitting BC03 models with exponentially declining star formation histories to the full spectral energy distributions (SEDs) confirms that the red galaxies are on average $\sim$1 Gyr old ($z_{\rm form} \sim 3.3$), contain little ongoing star formation, and span a stellar mass range of $M_* = (0.1$–$5) \times 10^{11}\ M_\odot$. In contrast, blue overdensity galaxies ($J_1 - H_l < 1.6$) are best fit by $\sim$0.1 Gyr BC03 models and have masses $M_* = 10^8$–$10^{10}\ M_\odot$.

We find candidate "brightest cluster galaxies" (BCGs) in each overdensity, with relatively large stellar masses: $M_*^{\rm A} = 3 \times 10^{11}$, $M_*^{\rm B} = 1 \times 10^{11}$, and $M_*^{\rm C} = 1 \times 10^{11}\ M_\odot$. As shown in Figure 4, BCG A is a quiescent "red and dead" galaxy, while BCGs B and C may contain recent star formation. A close inspection of BCGs A and B in Figure 2 suggests that they also have distinct structural properties: the latter is compact[10] ($r_e = 2^{+0.3}_{-0.5}$ kpc) while the former has a larger core ($r_e = 3^{+0.5}_{-0.5}$ kpc) plus an extended diffuse stellar halo. With 3–4 satellites within $r \sim 30$ kpc, we speculate BCG B will undergo a series of mergers and perhaps "puff up" in size (Hopkins et al. 2010). Clearly, we are probing an epoch where even some of the most

[10] As measured on the K_s-band FourStar image using two-dimensional Sérsic models fitted with `ISHAPE`, which is specifically designed to measure sizes of partially resolved objects (Larsen 1999).

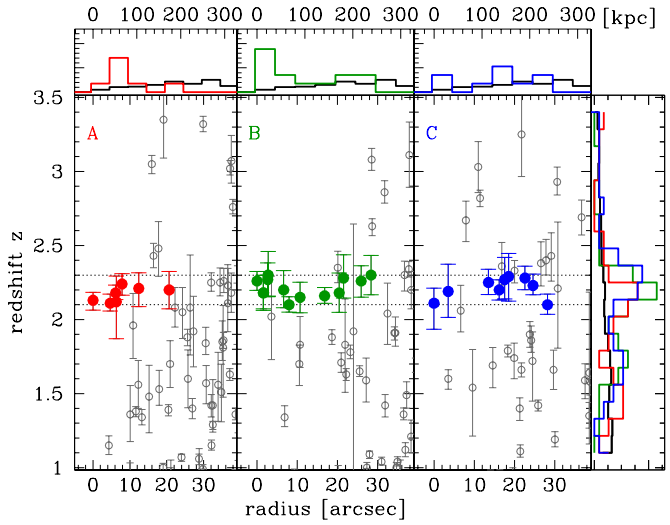

Figure 3. Photometric redshift against radial distance to the central brightest galaxy in the labeled overdensities ABC from Figure 1. Colored points and histograms are galaxies with $r < 30''$ and $2.1 \leqslant z \leqslant 2.3$. The histograms are normalized by the area from which the sample was drawn. The control histograms (black) in the top panels are the cumulative spatial distribution around all $z = 2.1$–2.3 galaxies. The control histograms in the right panel are all galaxies in the field. The overdensities show concentrated surface densities and peaked redshift distributions compared to the control samples.

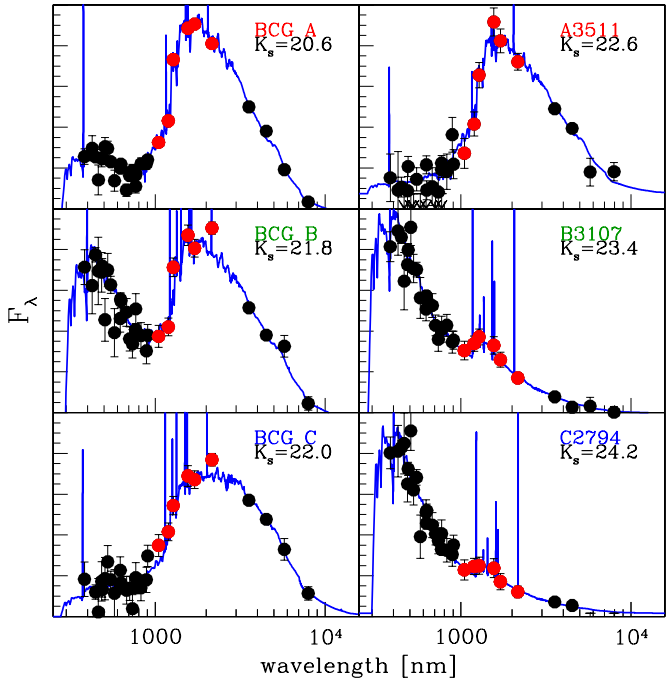

Figure 4. Observed 32-band SEDs of the central brightest galaxies (BCGs) in the overdensities (left panels) and randomly selected overdensity members (right panels). The highlighted red points are our custom FourStar filters, sensitive to near-IR light at 1.0–1.8 μm. The higher resolution spectral sampling of the SEDs in this range allows us to pinpoint the Balmer/4000 Å break as it shifts through medium-bandwidths $1.5 < z < 3.5$. Overplotted are the best-fit EAZY photometric redshift templates (blue). BCG A has a quiescent stellar population, while BCGs B and C have some star formation, including enhanced K_s-band flux likely due to Hα emission.

massive galaxies in the highest density regions were still forming a significant fraction of their stars (e.g., Glazebrook et al. 2004; van Dokkum & van der Marel 2007; Eisenhardt et al. 2008; Tran et al. 2010).

4.2. Comparison to Known High-z Overdensities

To help us interpret the $z = 2.2$ overdensities, we will now characterize various global properties of the overdensities and compare them to known high-redshift galaxy clusters and protoclusters.

As shown in Figure 1, the individual $z = 2.2$ overdensities have spatial extents of $r = 30''$ or 250 kpc. The galaxy clusters at $z \gtrsim 1.6$ show similar projected compact sizes (Andreon et al. 2009; Papovich et al. 2010; Tanaka et al. 2010; Gobat et al. 2011). Notably, the $z = 1.62$ cluster (Papovich et al. 2010; Tanaka et al. 2010) shows two galaxy clumps or subclusters over a region of $\sim 1'$. This is not unlike the configuration discussed here. In contrast, known protoclusters at $z \gtrsim 2$ are typically more diffuse, with lower overdensities and $\sim 8\times$ larger sizes (Steidel et al. 2000; Venemans et al. 2007). Indeed, overdensities A and B each show core surface densities of $\gtrsim 50$ galaxies arcmin^{-2}, with 5–6 members at $r \lesssim 10''$.

To estimate the total halo mass ($M_{\rm halo}$) of each overdensity, we use the relation between M_* and $M_{\rm halo}$ at $z = 2.2$ from the halo occupancy distribution analysis of Moster et al. (2010) and apply these to the M_* of the central BCGs. Although the uncertainties involved in converting stellar mass to halo mass are significant, we estimate that the overdensities have $M^{\rm A}_{\rm halo} \approx 6 \times 10^{13}$, $M^{\rm B}_{\rm halo} \approx 1 \times 10^{13}$, and $M^{\rm C}_{\rm halo} \approx 1 \times 10^{13}\ M_\odot$. The $M_{\rm halo}$ of A is in the same range as estimates for the $z = 2.07$ cluster (Gobat et al. 2011). Using a 1 Gpc^3 cosmological simulation (GiggleZ; G. B. Poole et al. 2012, in preparation; 2160^3 particles, WMAP5 cosmology; Komatsu et al. 2009), we find that $z = 2.2$ simulated halos with these masses will grow into $z = 0$ halos with mean masses of $M_{\rm halo} \sim (0.5$–$5) \times 10^{14}\ M_\odot$.

The detection of diffuse X-ray emission would provide independent confirmation of the existence of a deep gravitational potential well. We find no diffuse X-ray emission at the locations of the $z = 2.2$ overdensities in the COSMOS 55 ks *XMM-Newton* and 200 ks *Chandra* legacy images (Hasinger et al. 2007; Elvis et al. 2009; Cappelluti et al. 2009) to a point-source 0.5–2 keV sensitivity limit of $\sim 2 \times 10^{-15}$ and 2×10^{-16} erg cm^{-2} s^{-1}, respectively. The *XMM-Newton* flux limit corresponds to an X-ray luminosity upper limit of 7×10^{43} erg s^{-1}, similar to the value estimated for the extended emission around the $z = 2.07$ (Gobat et al. 2011) cluster.

Overall, the newly discovered $z = 2.2$ overdensities show a number of characteristics (e.g., $M_{\rm halo}$ estimates, presence of evolved massive galaxies, compact spatial distribution) similar to spectroscopically confirmed galaxy clusters at $1.5 < z < 2.1$ (Papovich et al. 2010; Tanaka et al. 2010; Gobat et al. 2011). Even so, there are also marked variations: e.g., overdensity C contains mostly blue star-forming galaxies, more resembling our field population at $z = 2.1$–2.3. Given the overall resemblance and the close proximity of the three overdensities on the sky, we consider it likely that all three overdensities may be part of a single forming massive cluster.

As shown in Figure 1, the region surrounding the $z = 2.2$ system contains several less-significant galaxy overdensities, as one might expect to find around a large overdensity (e.g., Springel et al. 2006). The overdensity just to the north of the $z = 2.2$ system is particularly interesting: it contains two $M_* \approx (1$–$5) \times 10^{11}\ M_\odot$ evolved galaxies separated by just $20''$.

5. DISCUSSION AND CONCLUSIONS

Using the first data from the Magellan/FourStar Galaxy Evolution Survey (Z−FOURGE), we have detected in the

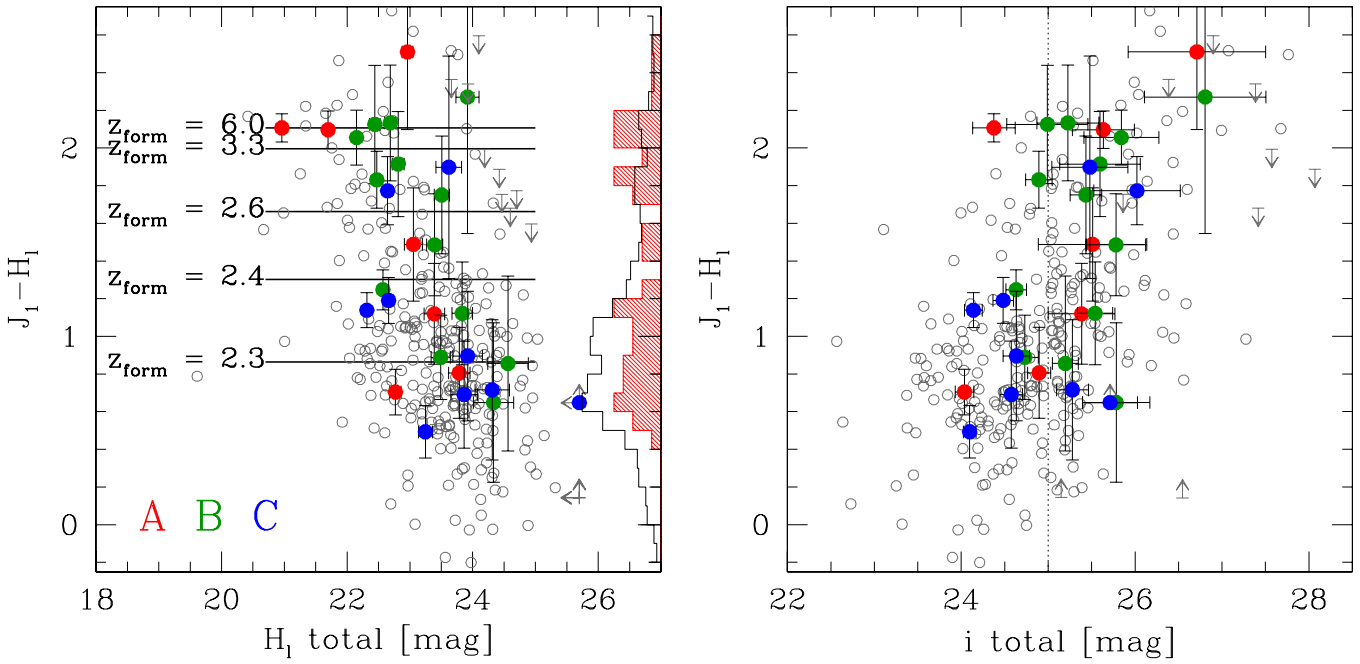

Figure 5. $J_1 - H_l$ vs. H_l (left panel) and vs. i (right panel) color–magnitude diagrams. Gray points and open histograms are for all 313 galaxies with $2.1 \leqslant z \leqslant 2.3$. Galaxy overdensity members are shown with the colored points and red hatched histograms. Histograms are arbitrarily normalized. Limits correspond to 2σ near-IR limiting depths. The overdensities have a higher fraction of red galaxies compared to the field. In the left panel, black lines show the $z = 2.2$ redshifted Bruzual & Charlot (2003) single-burst model predictions with solar metallicity and a Chabrier (2003) initial mass function for various ages or formation redshifts ($z_{\rm form}$; computed with `EzGal`, http://www.mancone.net/ezgal). In the right panel, red galaxies are generally very faint in the optical i band. For example, 80% of galaxies redder than $J_1 - H_l > 1.6$ are fainter than $i = 25$ (dotted line).

COSMOS field the most distant example of strong galaxy overdensities with red galaxies. The system at $z = 2.2$ extends $r \sim 1\farcm5$ on the sky and appears to be made up of multiple subcomponents, including two overdensities detected at $\gtrsim 20\sigma$ above the mean and another at $\sim 10\sigma$. The two strongest overdensities, A and B, each resemble spectroscopically confirmed galaxy clusters at $z \gtrsim 1.6$ (Papovich et al. 2010; Tanaka et al. 2010; Gobat et al. 2011): they contain significant populations of evolved galaxies (mean stellar age $\sim$1 Gyr or $z_{\rm form} \sim 3.3$) in a compact spatial distribution (<250 kpc) embedded in massive halos of $M_{\rm halo} \sim (1\text{–}6) \times 10^{13}\ M_\odot$.

Perhaps the most outstanding feature of the aggregate system is that it consists of multiple distinct galaxy overdensities in close spatial configuration. Whether the three $z = 2.2$ overdensities are a single gravitationally bound structure is not clear. Ultimately, high-precision spectroscopic redshifts of this structure are needed to confirm its existence and measure its velocity dispersion. Still, even if each overdensity is confirmed with spectroscopy, they could still be unbound and coupled to the Hubble flow. In this case, they possibly trace a filament in the dark matter density field and may evolve into a large-scale structure at $z = 0$, e.g., a supercluster (Geller & Huchra 1989).

To help us interpret the $z = 2.2$ system as a whole, we searched for analogs in the 1 Gpc^3 GiggleZ cosmological simulation (G. B. Poole et al. 2012, in preparation; see Section 4.2) by running 2 million random lines of sight (each a cylinder with 0.7 Mpc radius and 50 Mpc length to match the 2σ redshift uncertainty, $2\sigma_z \approx 0.06$, of the overdensities). If a three-halo system matching the set of overdensity $M_{\rm halo}$ estimates is found, then 98% of the time two or three of these halos will merge into a $z = 0$ cluster with $M_{\rm halo} \sim 10^{14}$–$10^{15}\ M_\odot$. At $z = 2.2$ in the simulation, these two- and three-halo systems show typical maximum separations of $\sim$0.9–1.8 Mpc three dimensions from their mean positions. Although this comparison is limited by the preliminary halo masses of the $z = 2.2$ overdensities, these results may suggest that there is high probability that two or more of the $z = 2.2$ overdensities will merge by $z = 0$.

If two or more of the overdensities are currently gravitationally bound, we may be viewing merging subclusters that are each in different evolutionary stages, including some whose galaxies are rapidly evolving and only just forming their red galaxy population (e.g., overdensity C). Perhaps this signifies the system is in a transitional phase between the known $z \gtrsim 2$ "protoclusters" (e.g., Steidel et al. 2005) with more diffuse distributions of blue galaxies, and the lower-redshift galaxy clusters with prominent red sequences. Of course, protocluster observations have largely been optically based, thus deep near-IR observations of such structures and deep optical spectroscopy of our candidate cluster are needed to understand the relationship between the various structures at $z \gtrsim 1.5$.

The discovery of the $z = 2.2$ system demonstrates the powerful combination of near-IR medium-bandwidth filters and deep imaging of the Z−FOURGE survey. These systems were undetectable in earlier optical and near-IR catalogs. For example, in the optically selected ($i < 25$) catalog of Ilbert et al. (2009), the overdensity is completely absent in our redshift slice of interest ($z = 2.1$–2.3). The relatively bright optical limit of this catalog means evolved galaxies at these redshifts are missed entirely (only two of our red overdensity galaxies have $i_{\rm total} < 25$, see Figure 5). Even with the K-band selected NMBS catalog of Whitaker et al. (2011), only a weak overdensity is seen in Figure 1, as the majority of the $z = 2.2$ overdensity galaxies are too faint to be detected in the 1.3 mag shallower NMBS.

The first results of the Z−FOURGE survey suggest that we are reaching a critical threshold in our ability to study

galaxy evolution as a function of local environment at $z \gtrsim 1.5$. By combining the spatial distribution with improved redshift information from deep medium-band filters in the near-IR, we can start to correlate the properties of K_s-selected galaxies with their environment, something that has so far only been done in detail for Lyman break galaxies (e.g., Steidel et al. 2000).

We acknowledge the Cook's Branch Conservancy for the gracious hospitality and comfortable surroundings which permitted the discovery of this exciting system. We are grateful to the FourStar instrumentation team and staff at LCO. We appreciate the useful comments from the anonymous reviewer. L.R.S. acknowledges funding from a Australian Research Council (ARC) Discovery Program (DP) grant DP1094370 and Access to Major Research Facilities Program which is supported by the Commonwealth of Australia under the International Science Linkages program. G.B.P. acknowledges support from two ARC DP programs (DP0772084 and DP1093738). C.P., K.V.T., and V.T. acknowledge support from National Science Foundation grant AST-1009707. Australian access to the Magellan Telescopes was supported through the National Collaborative Research Infrastructure Strategy of the Australian Federal Government.

Facility: Magellan:Baade (FourStar)

REFERENCES

Andreon, S., Maughan, B., Trinchieri, G., & Kurk, J. 2009, A&A, 507, 147
Bertin, E., & Arnouts, S. 1996, A&AS, 117, 393
Brammer, G. B., van Dokkum, P. G., & Coppi, P. 2008, ApJ, 686, 1503
Bruzual, G., & Charlot, S. 2003, MNRAS, 344, 1000
Capak, P. L., Riechers, D., Scoville, N. Z., et al. 2011, Nature, 470, 233
Cappelluti, N., Brusa, M., Hasinger, G., et al. 2009, A&A, 497, 635
Chabrier, G. 2003, PASP, 115, 763
Croton, D. J., Springel, V., White, S. D. M., et al. 2006, MNRAS, 365, 11
Eisenhardt, P. R. M., Brodwin, M., Gonzalez, A. H., et al. 2008, ApJ, 684, 905
Elvis, M., Civano, F., Vignali, C., et al. 2009, ApJS, 184, 158
Fassbender, R., Nastasi, A., Böhringer, H., et al. 2011, A&A, 527, L10
Geller, M. J., & Huchra, J. P. 1989, Science, 246, 897
Glazebrook, K., Abraham, R. G., McCarthy, P. J., et al. 2004, Nature, 430, 181
Gobat, R., Daddi, E., Onodera, M., et al. 2011, A&A, 526, 133
Hasinger, G., Cappelluti, N., Brunner, H., et al. 2007, ApJS, 172, 29
Hopkins, P. F., Bundy, K., Hernquist, L., Wuyts, S., & Cox, T. J. 2010, MNRAS, 401, 1099
Ilbert, O., Capak, P., Salvato, M., et al. 2009, ApJ, 690, 1236
Komatsu, E., Dunkley, J., Nolta, M. R., et al. 2009, ApJS, 180, 330
Kriek, M., van Dokkum, P. G., Labbé, I., et al. 2009, ApJ, 700, 221
Larsen, S. S. 1999, A&AS, 139, 393
McCarthy, P. J., Yan, H., Abraham, R. G., et al. 2007, ApJ, 664, L17
Moster, B. P., Somerville, R. S., Maulbetsch, C., et al. 2010, ApJ, 710, 903
Papovich, C. 2008, ApJ, 676, 206
Papovich, C., Momcheva, I., Willmer, C. N. A., et al. 2010, ApJ, 716, 1503
Persson, S. E., Barkhouser, R., Birk, C., et al. 2008, Proc. SPIE, 7014, 95
Santos, J. S., Fassbender, R., Nastasi, A., et al. 2011, A&A, 531, L15
Scoville, N., Aussel, H., Brusa, M., et al. 2007, ApJS, 172, 1
Springel, V., Frenk, C. S., & White, S. D. M. 2006, Nature, 440, 1137
Springel, V., White, S. D. M., Jenkins, A., et al. 2005, Nature, 435, 629
Steidel, C. C., Adelberger, K. L., Shapley, A. E., et al. 2000, ApJ, 532, 170
Steidel, C. C., Adelberger, K. L., Shapley, A. E., et al. 2005, ApJ, 626, 44
Tanaka, M., Finoguenov, A., & Ueda, Y. 2010, ApJ, 716, L152
Tran, K. H., Papovich, C., Saintonge, A., et al. 2010, ApJ, 719, L126
van Dokkum, P. G., Labbé, I., Marchesini, D., et al. 2009, PASP, 121, 2
van Dokkum, P. G., & van der Marel, R. P. 2007, ApJ, 655, 30
Venemans, B. P., Röttgering, H. J. A., Miley, G. K., et al. 2007, A&A, 461, 823
Whitaker, K. E., Labbé, I., van Dokkum, P. G., et al. 2011, ApJ, 735, 86
Wolf, C., Meisenheimer, K., Rix, H., et al. 2003, A&A, 401, 73